ELSEVIER

Fusion Engineering and Design 27 (1995) 536–543

Fusion Engineering and Design

Mechanical response and fatigue analysis of the first wall structure of the PROMETHEUS IFE reactor

A. El-Azab, N.M. Ghoniem

Mechanical, Aerospace and Nuclear Engineering Department, 46-147G Eng. IV, University of California, Los Angeles, Los Angeles, CA 90095, USA

Abstract

Analysis of the mechanical response of the PROMETHEUS inertial fusion energy (IFE) reactor first wall is presented. Time-dependent stress, strain and displacement fields are numerically determined for an SiC–SiC composite first wall structure, in response to two types of pulsed loadings. These are ablation momentum associated with sudden evaporation of the protecting liquid metal film due to X-ray deposition and the interaction of the first wall with the induced pressure shock waves during cavity heat up and cool down phases. Based on these results, a modular first wall concept is recommended. Fatigue life time calculations based on residual stiffness and damage evolution criteria for the SiC–SiC composite first wall structure are presented.

1. Introduction

During operation, the first wall of an inertial fusion energy (IFE) reactor is usually subjected to pulsed thermo-mechanical loading. The life-time of the first wall is determined by the protecting scheme against the X-ray and debris resulting from pellet implosion, high-temperature corrosion-fatigue interaction, radiation damage and thermo-mechanical fatigue damage. Excellent protection schemes have been suggested to prolong the life-time of the first wall structure by including sacrificial layers of materials which evaporate following pellet implosion due to instantaneous deposition of large amounts of energy on the surface. Liquid films of varying thickness (fractions of a millimeter up to a centimeter) are usually used [1]. Lithium, lithium–lead and lead films are proposed as primary candidates based on neutron multiplication, tritium breeding and cavity hydrodynamics considerations. In the PROMETHEUS IFE reactor [2,3], liquid lead film of 0.5 mm thickness is used in a wetted wall design concept. The choice of SiC–SiC composite as a structural material for the first wall (and blanket) offers the required high-temperature stability against corrosive actions of liquid lead coolant and the protecting liquid lead film, as well as meeting the safety and environmental goals of fusion energy. SiC is also known for its low activation characteristics and radiation damage resistance.

In the wetted wall design concept which is chosen for the PROMETHEUS IFE reactor [2,3], early deposition of X-rays, which carry about 7% of the target yield, results in an instantaneous partial ablation of the protecting liquid film. Consequently, the first wall structure is subjected to a mechanical impulse almost at the instant of the microexplosion. Sudden evaporation of the protecting lead film creates pressure shock waves which start at the first wall and propagate to the center of the cavity.

0920-3796/95/$09.50
SSDI 0920-3796(94)00120-1

To analyze the fatigue life of the first wall, the time history of the gas pressure at the first wall, which determines the time-dependent first wall loading following the microexplosion must be calculated. Detailed hydrodynamics modeling of the pellet implosion, energy yield distribution and the interaction with cavity vapor is required to determine the pressure history at the first wall [1–3]. As a result of the initial impulse and subsequent shock wave reflections, the first wall undergoes time-dependent displacements. The associated stresses can be determined by studying the dynamic response of the first wall, which depends on the mechanical attachment, size, density and thickness of first wall modules. Owing to the time-dependent nature of the induced stresses, it is essential to include fatigue life-time analysis in designing the first wall of an IFE reactor.

In order to assess the fatigue characteristics, detailed structural response computational codes which are based on finite element computations are usually used to extract critical stress or strain amplitudes. However, some fatigue parameters, such as maximum stress level and frequency can reasonably be estimated using analytical or finite difference methods. These methods can also be used to compare different design concepts, e.g. continuous vs. segmented (modular) first wall designs. In the present analysis, the equation of motion is solved for the first wall of the PROMETHEUS IFE reactor and the magnitude and frequency of maximum stresses are determined, as basic fatigue data. The finite difference technique is used to solve the time-dependent biharmonic displacement equation associated with plate dynamics. A discussion of specific results which enable the choice of the first wall final configuration is presented. Finally, an assessment of first wall fatigue life is discussed.

2. First wall loading

As mentioned before, the first wall is subjected to an ablation momentum as a result of early deposition of X-rays at the instant of the pellet implosion, followed by a time-dependent pressure loading associated with shock wave reflections at the first wall. The initial ablation momentum is introduced in the mechanical model as an initial velocity of the structure at each pellet implosion by applying the principle of conservation of momentum. For a total impluse I, uniformly distributed over the surface, the initial velocity v_0 is given by

$$v_0 = \frac{1}{\rho h}\left(\frac{dI}{dA}\right) = \frac{I}{\rho A h} \tag{1}$$

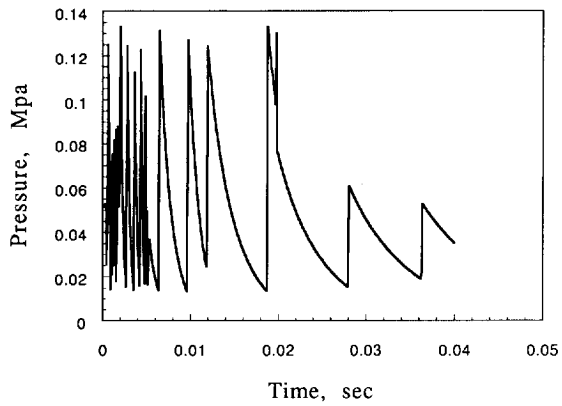

Fig. 1. The history of pressure at PROMETHEUS IFE reactor following pellet explosion.

where ρ is the effective density of the structure, h is its thickness and A is the total surface area. Typical ablation momentum impulse for the PROMETHEUS IFE reactor is found to be 3.17×10^3 N s [2] for the pellet parameters used in that study. A typical time variation of the local pressure at the first wall is shown in Fig. 1 for a base case of 5 m cavity radius. This figure shows that the pressure loading of the first wall diminishes effectively before the next microexplosion takes place (repetition rate 5.65 and 3.5 explosions per second for the PROMETHEUS-L and PROMETHEUS-H respectively).

3. Spherical shell model

For a preliminary estimate of fatigue parameters of the cavity, a spherical shell model is considered ($R = 5$ m, $h = 1$ cm). The equation of motion is written as

$$\frac{d^2u}{dt^2} + \omega^2 u = \frac{P(t)}{\rho h} \tag{2}$$

where u is the radial displacement, $\omega = 2\pi/T = (2E/\rho R^2)^{1/2}$ is the frequency of vibration, E is Young's modulus and $P(t)$ is the time-dependent pressure (assumed uniform). For SEP SiC–SiC composites the elastic modulus E is 200 GPa at 1000 °C. The corresponding natural period T is found to be 2.5×10^{-3} s. The time-dependent hoop stress $\sigma(t)$ in the spherical shell is given by

$$\sigma(t) = E\frac{u(t)}{R} \tag{3}$$

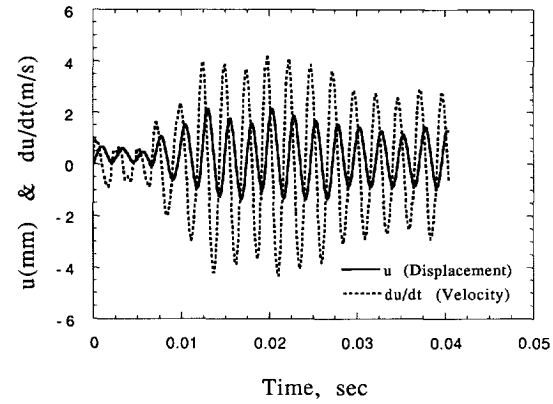

Fig. 2. Instantaneous velocity and radial dsiplacement of the continuous (spherical shell) first wall.

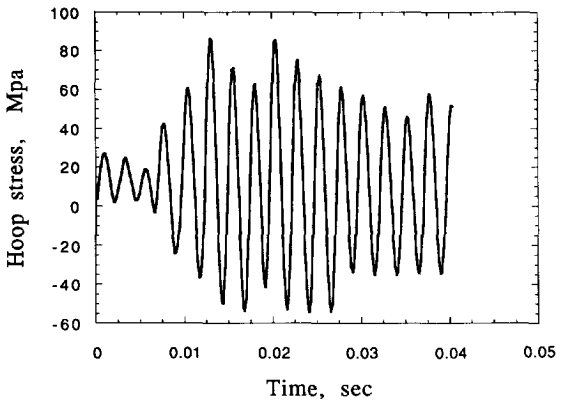

Fig. 3. Hoop stress history in the continuous first wall.

Although the equation of motion (2) can be solved analytically, it is integrated numerically in the present analysis since the pressure loading cannot be accurately fitted to a suitable function of time. The initial conditions are given by $u(0) = 0$ for the displacement and $du(0)/dt = v_0$ which is determined by Eq. (1). The displacement and radial velocity of the vibrating shell are shown in Fig. 2. The hoop stress is shown in Fig. 3. It is of interest to note that the difference Δu between the maximum and minimum radial displacement is $\Delta u \sim 3.5$ mm and the corresponding stress difference is $\Delta\sigma \sim 100-140$ MPa at steady state. These values are not acceptable from the structural design point of view. Fig. 4 shows the time-dependent kinetic energy of the vibrating wall. The conclusions that should be emphasized at this level of analysis can be summarized as follows.

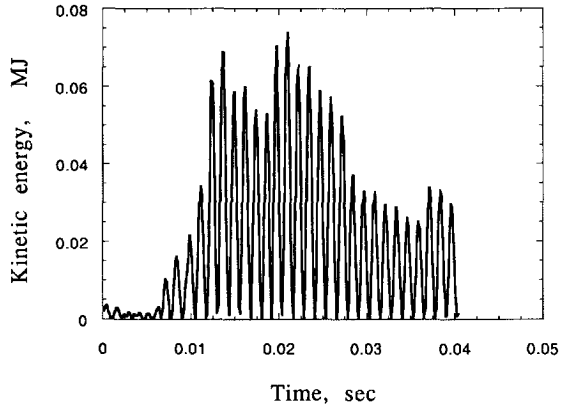

Fig. 4. Kinetic energy of the continuous first wall.

(1) To avoid high stresses, segmentation of the first wall is preferable. Integration of the first wall with the blanket is also a reasonable design approach since it will constrain the vibration of the first wall.
(2) Because of the high velocity of the vibrating first wall, the stability of the protecting film is concluded to be an important issue.
(3) The maximum kinetic energy of the vibrating wall is 0.07 MJ compared with pellet yield of 655 MJ. This suggests that no damping mechanism is required.

4. Modular first wall

The first wall of the PROMETHEUS IFE reactor consists of plate panels of rectangular shape which are made of a tubular structure containing the first wall coolant. These panels are mechanically attached to the underlying blanket structure. In this way the first wall acts as a stiffened plate subject to the ablation and the pressure loading as a result of the pellet explosion, given that buckling is not experienced in the side walls of the blanket itself. The panel size and method of support are determined by two factors: (1) the requirement that the maximum stress must be below its design limit and (2) the maintenance scheme. The overall thickness of these panels is 6 cm and the plate dimensions are 1×1.5 m^2. A schematic representation of the first wall/blanket arrangement is shown in Fig. 5(a) and the plate model of the first wall is shown in Fig. 5(b). The effective plate thickness could be less than 6 cm because the liquid lead inside the first wall tubes would not offer any flexural rigidity. Moreover, the presence of liquid lead within the first wall provides large inertial

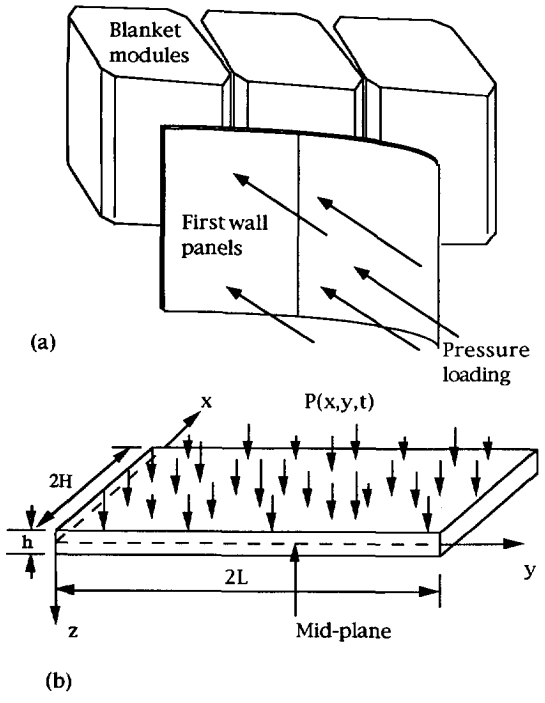

Fig. 5. Schematic of (a) the first wall/blanket configuration and (b) the plate model of the PROMETHEUS first wall.

effects to the first wall since it is heavier than the SiC structure itself. Hence, we expect that the results underestimate the magnitude of the stresses throughout the plate.

The plate representing the combined first wall/blanket integrated structure is treated as an orthotropic material since SEP 2D SiC–SiC composite [4] is used. The equation of motion governing the out-of-plane displacement $u(x, y, t)$ is given by

$$D_1 \frac{\partial^4 u}{\partial x^4} + 2D_3 \frac{\partial^4 u}{\partial x^2 \partial y^2} + D_2 \frac{\partial^4 u}{\partial y^4} + \rho h \frac{\partial^2 u}{\partial t^2} = P(x, y, t) \quad (4)$$

where D_1, D_2 and D_3 are the orthotropic flexural rigidity coefficients and ρh is the effective mass per unit area of first wall panel. Eq. (4) assumes that mid-plane symmetry exists. It also assumes zero transverse shear across the plate thickness (i.e. $\varepsilon_{xz} = \varepsilon_{yz} = 0$). The orthotropic bending rigidity coefficients are given by

$$D_1 = \frac{E_1 h^3}{12(1 - \nu_{12}\nu_{21})}$$

$$D_2 = \frac{E_2 h^3}{12(1 - \nu_{12}\nu_{21})}$$

$$D_3 = D_{12} + 2D_{66} \quad (5)$$

where E_1 and E_2 are the Young's moduli in the x and y directions respectively, ν_{ij} are the Poisson ratios and D_{12} and D_{66} are given by

$$D_{12} = \nu_{21} D_1 = \nu_{12} D_2$$

$$D_{66} = \frac{G_{12} h^3}{12} \quad (6)$$

in which G_{12} is the shear modulus in the plane of the panel. For SEP 2D SiC–SiC composite, $E_1 = E_2 = 200$ GPa, $G_{12} = 120$ GPa, $\nu_{12} = \nu_{21} = 0.15$, and $\nu_{13} = 0.4$. The density of the composite is $\rho = 2500$ kg m^{-3} [4].

The in-plane stresses can then be recovered from the out-of-plane displacement as follows

$$\sigma_x = [Q_{11}\kappa_x + Q_{12}\kappa_y]z$$

$$\sigma_y = [Q_{12}\kappa_x + Q_{22}\kappa_y]z$$

$$\sigma_{xy} = 2Q_{66}\kappa_{xy} z \quad (7)$$

where Q_{ij} are the stiffness coefficients of the composite material, z is the distance through the thickness measured from the mid-plane of the plate, as shown in Fig. 5, and κ_x, κ_y and κ_{xy} are given by

$$\kappa_x = -\partial^2 u/\partial x^2 \quad \kappa_y = -\partial^2 u/\partial y^2 \quad \kappa_{xy} = -\partial^2 u/\partial x\, \partial y \quad (8)$$

The stiffness coefficients Q_{ij} are given by

$$Q_{11} = E_1/(1 - \nu_{12}\nu_{21})$$

$$Q_{22} = E_2/(1 - \nu_{12}\nu_{21})$$

$$Q_{12} = Q_{21} = \nu_{21}E_1/(1 - \nu_{12}\nu_{21}) = \nu_{12}E_2/(1 - \nu_{12}\nu_{21})$$

$$Q_{66} = G_{12} \quad (9)$$

The initial conditions are written as

$$u(x, y, 0) = 0 \qquad \dot{u}(x, y, 0) = v_0 \quad (10)$$

where v_0 is determined by Eq. (1). The plate is considered to be clamped at four sides. Assuming the dimensions of the plate are $2H$ and $2L$ along the x and y directions respectively, and taking the center of the coordinate system to be the plate center, the boundary conditions can be written as

$$u(x, \pm L, t) = u(y, \pm H, t) = 0$$

$$\frac{\partial u(x, \pm L, t)}{\partial y} = \frac{\partial u(y, \pm H, t)}{\partial x} = 0 \quad (11)$$

5. Numerical solution of the out-of-plane displacement equation

The out-of-plane displacement equation is solved by a finite difference technique [6], where Euler's forward difference scheme is used for the time derivative and a centered finite difference scheme is employed for spatial derivatives of the displacement. The displacement $u(x, y, t)$ is approximated by the discretized displacement $u(i, j, k)$. The time step is denoted by Δt and the spatial increments along the x and y directions are denoted by Δx and Δy respectively. The time derivative in Eq. (4) is then given by

$$\frac{\partial^2 u}{\partial t^2} \approx \frac{u(i,j,k) + u(i,j,k-2) - 2u(i,j,k-1)}{(\Delta t)^2} \tag{12}$$

The spatial derivatives are also written as

$$\frac{\partial^4 u}{\partial x^4} \approx \frac{1}{(\Delta x)^4}\{6u(i,j,k) - 4[u(i+1,j,k) + u(i-1,j,k)] + u(i+2,j,k) + u(i-2,j,k)\}$$

$$\frac{\partial^4 u}{\partial y^4} \approx \frac{1}{(\Delta y)^4}\{6u(i,j,k) - 4[u(i,j+1,k) + u(i,j-1,k)] + u(i,j+2,k) + u(i,j-2,k)\}$$

$$2\frac{\partial^4 u}{\partial x^2 \partial y^2} \approx \frac{2}{(\Delta x \Delta y)^2}\{4u(i,j,k) + u(i+1,j+1,k) + u(i+1,j-1,k) + u(i-1,j+1,k) + u(i-1,j-1,k) - 2[u(i,j+1,k) + u(i+1,j,k) + u(i,j-1,k) + u(i-1,j,k)]\} \tag{13}$$

Substituting Eqs. (12) and (13) in Eq. (4) and arranging terms, the final form of the discretized equation can be written as

$$\left[C_1 + \frac{\rho h}{(\Delta t)^2}\right]u(i,j,k) + C_2[u(i+1,j,k) + u(i-1,j,k)] + C_3[u(i,j+1,k) + u(i,j-1,k)] + C_4[u(i+1,j+1,k) + u(i+1,j-1,k) + u(i-1,j+1,k) + u(i-1,j-1,k)] + C_5[u(i+2,j,k) + u(i-2,j,k)] + C_6[u(i,j+2,k) + u(i,j-2,k)] = P(i,j,k) - \frac{\rho h}{(\Delta t)^2}[u(i,j,k-2) - 2u(i,j,k-1)] \tag{14}$$

where the constants C_1 through C_6 are given by

$$C_1 = \frac{6D_1}{(\Delta x)^4} + \frac{6D_2}{(\Delta y)^4} + \frac{8D_3}{(\Delta x \Delta y)^2}$$

$$C_2 = -\frac{4D_1}{(\Delta x)^4} - \frac{4D_3}{(\Delta x \Delta y)^2}$$

$$C_3 = -\frac{4D_2}{(\Delta y)^4} - \frac{4D_3}{(\Delta x \Delta y)^2}$$

$$C_4 = \frac{2D_3}{(\Delta x \Delta y)^2}$$

$$C_5 = \frac{D_1}{(\Delta x)^4}$$

$$C_6 = \frac{D_2}{(\Delta y)^4} \tag{15}$$

The solution to the problem is completed by casting the discretized Eq. (14) into a matrix form, where the unknown vector represents nodal displacements. A Gaussian elimination technique is used to solve the resulting matrix equation at each time step. Nodal velocities of the vibrating plate are found by calculating the ratio $[u(i,j,k) - u(i,j,k-1)]/\Delta t$ for each nodal point. Stresses are recovered using Eq. (7). The instantaneous displacement and velocity at the center of the PROMETHEUS IFE first wall plate are shown in Fig. 6 for the pressure loading shown in Fig. 1. The stress history at the center of the plate (for $z = \pm h/2$) is shown in Fig. 7. For clamped plates under bending conditions with uniform loading, the maximum stresses occur at the clamped edges ($x = \pm H$, $y = 0$, $z = \pm h/2$). Fig. 8 shows the stress history at that point. The fact that displacements, velocity and stresses all diminish before the next explosion takes place can be interpreted by the phase shift between the pressure shock wave

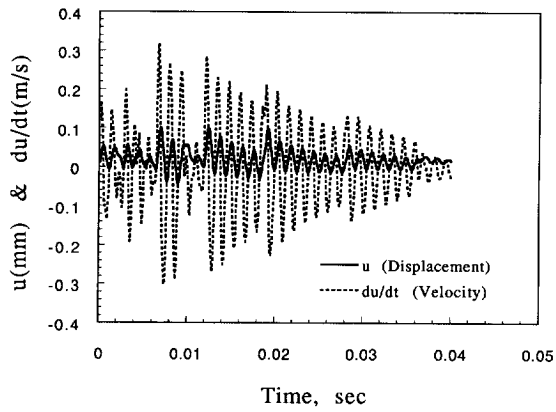

Fig. 6. Instantaneous velocity and displacement at the plate center.

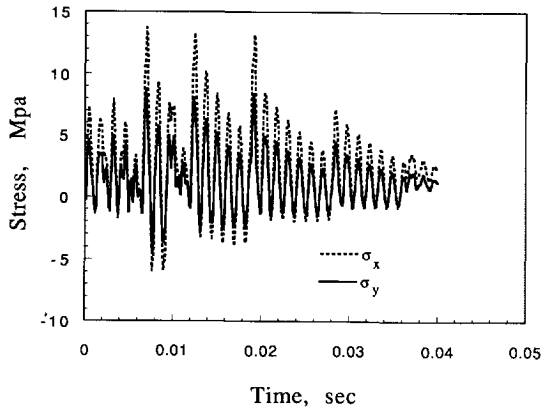

Fig. 7. Normal stress history at the center of the plate.

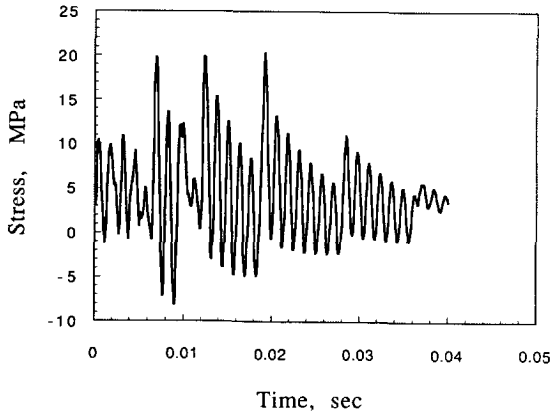

Fig. 8. History of stress at the plate edge.

reflections at the first wall and the velocity of the vibrating plate. For the given plate dimensions and mass density, the frequency of vibration is found to be approximately 800 Hz. It is also observed that resonance between the vibrating plate and the pressure loading is unlikely to occur. This is because, as the cavity cools down, the frequency and magnitude of the pressure loading of the first wall becomes smaller.

6. Fatigue life evaluation

The process of fatigue damage and failure in composites is highly complicated due to the fact that many types of local damage parameters are involved and the onset of failure is generally controled by the microstructure and fiber architecture, laminate lay up, loading configuration and environment. The composite damage involves matrix microcracking, interface debonding, fiber fracture and delamination. Different loading conditions may result in one or more of these damage mechanisms. Phenomenological damage evolution and failure under cyclic loading conditions are not easy to derive. Composite designers [7] have presented a systematic conceptual scheme for the evaluation of fatigue performance of composites based on certain damage mechanism maps called fatigue life diagrams, which are essentially different from the classical S–N method.

For composite laminates under fatigue loading, three types of phenomenological approach have been used so far to assess fatigue life. The first approach considers the residual strength degradation where failure is assumed to occur when the residual strength becomes equal to the maximum stress amplitude. Broutman and Sahu [8] proposed a cumulative damage theory based on a linear strength degradation equation. Hahn and Kim [9] introduced a non-linear residual strength degradation equation, which was further investigated by Yang and Liu [10]. The second approach considers modulus degradation and assumes that fatigue failure occurs when the modulus degrades to a certain level [11,12]. The third approach is based on damage tolerance of composite materials and assumes that fatigue failure occurs if the maximum global strain, resulting from stiffness loss associated with damage growth at a certain number of cycles, reaches the effective failure strain when local delamination forms [13]. This approach combines both residual strength degradation and modulus degradation by using the concept of strain energy release rate and delamination growth law.

Fig. 9 shows the stress–strain curve for SEP 2D SiC–SiC composites for the virgin vs. fatigue tested material. After 10^6 tensile–tensile cycles between 10 and 100 MPa, it can be shown that the upper characteristics were maintained. In order to use this data in fatigue life calculation for the PROMETHEUS IFE reactor first wall, we follow the approach of residual stiffness as developed by Bangyan and Lessard [14]. In this approach the residual stiffness is related to the number N of cycles, the maximum fatigue stress σ_{max}, and the ultimate stress σ_u by the following formula

$$\frac{E}{E_0} = 1 - KN^{2/(2+b)}\sigma_{\max}^{2b/(2+b)}\left(1 - \frac{\sigma_{\max}}{\sigma_u}\right) \tag{16}$$

where K and b are constants, which are to be determined from fatigue data of the material. According to Lacombe and Bonnet [6], and Fig. 9, the residual modulus is 180 GPa at 10^6 cycles at $\sigma_{max} = 100$ MPa. By taking $\sigma_u = 200$ MPa [6], and assuming $E/E_0 = 0.95$ at 100 cycles for the given maximum and ultimate

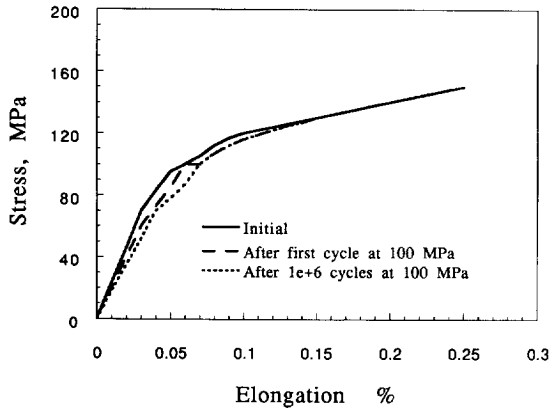

Fig. 9. Stress–strain diagram for SEP 2D SiC–SiC composite (fatigue-tested vs. virgin material). Data from Ref. [6].

stresses, the constants K and b are found to be $K = 1.9 \times 10^{-5}$ and $b = 12.3$. Now Eq. (16) can be applied using the stress information given in Fig. 8, for σ_x at the clamped plate edge. It is to be noted that the component $\sigma_y = 0$ along this edge. To be conservative, let us assume that the maximum stress level is always 20 MPa. Although the time-dependent stress at the clamped edge is tensile-compressive, the tensile part is dominant.

With $\sigma_u = 200$ MPa and the calculated values of K and b, the formula (16) can be simplified to $E/E_0 = 1 - 2.956 \times 10^{-3} N^{0.14}$, which is used to produce Fig. 10. Based on this figure it can be shown that for SEP SiC–SiC composites, a residual modulus which is 90% of the modulus of the virgin material is retained after three service years in the PROMETHEUS cavity, based on a vibration frequency of 800 Hz. Such residual modulus ratio is an acceptable limit for most ceramic matrix composites. It can be concluded here that the life-time of the first wall is not controled by mechanical fatigue damage, but rather by radiation effects on the structural properties of the SiC–SiC composite materials. The residual modulus E_f/E_0 at complete failure is determined by the condition that the global strain resulting from the siffness loss associated with damage growth reaches the static ultimate strain, i.e. $E_f/E_0 = \sigma_{max}/\sigma_u$ [14], which yields $E_f/E_0 = 20/200 = 0.1$. Based on Fig. 10, this limit occurs after several service years.

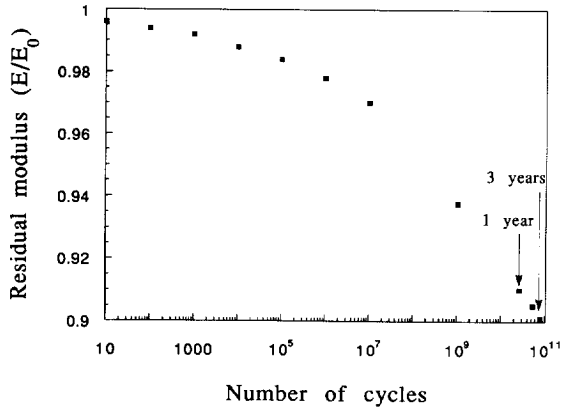

Fig. 10. Residual modulus vs. the number of cycles for PROMETHEUS first wall.

7. Summary

The out-of-plane displacement equation is solved for the SiC–SiC composite first wall of the PROMETHEUS IFE reactor, and the time varying stress history is evaluated. Residual stiffness is evaluated based on the stress history at the clamped edge of the first wall, with the simple phenomenological damage equation developed in [14]. It is found that the SEP 2D SiC–SiC composite retains 90% of its stiffness under the PROMETHEUS IFE reactor first wall conditions for three service years. Despite this conclusion, another aspect of fatigue damage must be thought of, that is the degradation of modulus in SiC–SiC composite which is a ceramic material associated with a certain density and distribution of matrix microcracks, interface debond cracks, and delamination cracks. The leak-tightness and sealing characteristics of the material will certainly be affected by these microcracks, thus making the bulk of the material accessible to the coolant, which may lead to further unknown material degradation.

Acknowledgment

This work was supported by the US Department of Energy under contract DE-AC02-90ER54101.

References

[1] L.A. Gleen and D.A. Young, Dynamic loading of the structural wall in a lithium-fall fusion reactor, Nucl. Eng. Des. 54 (1979) 1–16.

[2] M.S. Tillack, M.Z. Youssef, M.A. Abdou, A.R. Raffray, J. Eggleston, A. El-Azab, Z. Gorbis, F. Issacci, I. Jun, S. Sharafat, A.Y. Ying and N.M. Ghoniem, Initial design of the PROMETHEUS wetted wall IFE reactor cavity, UCLA-FNT-51 (1991).

[3] M.S. Tillack, M.Z. Youssef, M.A. Abdou, A.R. Raffray, J. Eggleston, A. El-Azab, Z. Gorbis, F. Issacci, I. Jun, S. Sharafat, A.Y. Ying and N.M. Ghoniem, Design and analysis of the PROMETHEUS wetted wall IFE reactor cavity, Proc. 14th IEEE/NPSS Symp. on Fusion Engineering, Vol. I (IEEE Service Center, 1991) pp. 223–226.

[4] A. Lacombe and C. Bonnet, Ceramic matrix composites, key materials for future space plane technology, Proc. AIAA Second Int. Aerospace Planes Conf. (AIAA, Inc., 1990) pp. 1–14.

[5] J.R. Vinson and R.L. Sierakowski, The Behavior of Structures Composed of Composite Materials, Kluwer, 1990, pp. 85–87.

[6] S.P. Timoshinko and J.N. Goodier, Theory of Elasticity, McGraw-Hill, 3rd edn., 1987, pp. 538–545.

[7] Ramesh Talerja, Fatigue of Composite Materials, Technometric, 1987, pp. 1–5.

[8] I.J. Broutman and S. Sahu, A new theory to predict cumulative fatigue damage in fiber glass reinforced plastics, in Composite Materials: Testing and Design (ASTM STP 497, Philadelphia, 1972) pp. 170–188.

[9] H.T. Hahn and R.Y. Kim, Proof testing of composite materials, J. Comp. Mater. 9 (1975) 297–311.

[10] J.N. Yang and M.D. Liu, Residual strength degradation model and theory of periodic proof test for graphite/epoxy laminates, J. Comp. Mater. 11 (1977) 176–203.

[11] H.T. Hahn and R.Y. Kim, Fatigue behavior of composite laminates, J. Comp. Mater. 10 (1976) 150–180.

[12] T.K. O'Brien and K.L. Reifsnider, Fatigue damage evaluation through stiffness measurements in boron-epoxy laminates, J. Comp. Mater. 15 (1981) 55–70.

[13] T.K. O'Brien, Characterization of delamination onset and growth in a composite laminate, in K.L. Reifsnider (ed.), Damage in Composite Materials (ASTP STP 775). (ASTM, Philadelphia, 1982) pp. 7–33.

[14] Bangian Liu and Larry B. Lesard, Fatigue and damage-tolerance analysis of composite laminates: stiffness loss, damage-modeling, and life prediction, Comp. Sci. Technol. 51 (1994) 43–51.